ARTICLES
https://doi.org/10.1038/s41550-021-01598-4

nature astronomy

Check for updates

Galaxies lacking dark matter produced by close encounters in a cosmological simulation

Jorge Moreno[1,2,3]✉, Shany Danieli[4,5], James S. Bullock[2], Robert Feldmann[6], Philip F. Hopkins[3], Onur Çatmabacak[6], Alexander Gurvich[7], Alexandres Lazar[2], Courtney Klein[2], Cameron B. Hummels[3], Zachary Hafen[2], Francisco J. Mercado[2], Sijie Yu[2], Fangzhou Jiang[3,8], Coral Wheeler[9], Andrew Wetzel[10], Daniel Anglés-Alcázar[11,12], Michael Boylan-Kolchin[13], Eliot Quataert[4], Claude-André Faucher-Giguère[7] and Dušan Kereš[14]

The standard cold dark matter plus cosmological constant model predicts that galaxies form within dark-matter haloes, and that low-mass galaxies are more dark-matter dominated than massive ones. The unexpected discovery of two low-mass galaxies lacking dark matter immediately provoked concerns about the standard cosmology and ignited explorations of alternatives, including self-interacting dark matter and modified gravity. Apprehension grew after several cosmological simulations using the conventional model failed to form adequate numerical analogues with comparable internal characteristics (stellar masses, sizes, velocity dispersions and morphologies). Here we show that the standard paradigm naturally produces galaxies lacking dark matter with internal characteristics in agreement with observations. Using a state-of-the-art cosmological simulation and a meticulous galaxy-identification technique, we find that extreme close encounters with massive neighbours can be responsible for this. We predict that ~30% of massive central galaxies (with at least 10^{11} solar masses in stars) harbour at least one dark-matter-deficient satellite (with 10^{8}–10^{9} solar masses in stars). This distinctive class of galaxies provides an additional layer in our understanding of the role of interactions in shaping galactic properties. Future observations surveying galaxies in the aforementioned regime will provide a crucial test of this scenario.

For over half a century, cold dark matter has been a key ingredient in our understanding of galaxy formation[1,2]. In the low-mass regime, the standard cold dark matter paradigm[3] predicts that galaxies should be more dark-matter dominated[4]. This is supported by observations in the nearby Universe[5]. For this reason, the detection of DF2 and DF4, two low-mass galaxies devoid of dark matter, was not anticipated[6,7]. This intriguing discovery immediately sparked several searches for numerical analogues in cosmological simulations[8–18], with limited success. Indeed, although idealised numerical experiments[19–23] had hinted at the possibility of the existence of such analogues within the standard model, no cosmological simulation had successfully generated numerical galaxies whose internal properties (stellar masses, velocity dispersions and morphologies) simultaneously matched those of their observed counterparts. Unsurprisingly, the absence of dark-matter-deficient low-mass galaxies in some of the earlier cosmological simulations also raised doubts about the validity of the standard paradigm itself[8,22]—although these studies did not conduct an exhaustive comparison with previous works (Supplementary Information). In this Article we demonstrate that a novel cosmological hydrodynamical simulation (which presupposes this paradigm) naturally creates adequate numerical versions of the observed dark-matter-deficient galaxies. This simulation utilised the Feedback In Realistic Environments (FIRE-2) physics model[24], which successfully reproduces an array of galaxy properties[25] and is state of the art in its ability to resolve the internal structure of individual galaxies within a large cosmological environment (see Methods for details). By direct comparison with observations, we confirm that one of our simulated galaxies resembles DF2 and DF4 in arresting ways. This finding alleviates the aforementioned concerns, and mitigates the exigency for alternative explanations invoking new (non-standard) physics, such as self-interacting dark matter[22] and modified gravity[8,26–30].

We identified seven galaxies lacking dark matter within a volume of $10^{4}\,\mathrm{Mpc}^{3}$. Figure 1 shows present-time images of the environments around these simulated dark-matter-deficient galaxies (white circles), which we name in honour of the seven Cherokee clans: Bird, Blue, Deer, Long Hair, Paint, Wild Potato and Wolf. The top-left panels show mock Hubble Space Telescope composite u/g/r stellar images (down to 28.9 mag arcsec^{-2}, corresponding to $10^{5}\,L_{\odot}\,\mathrm{kpc}^{-2}$, where $L_{\odot}$ is the luminosity of the Sun) and the bottom-left panels display corresponding dark-matter-mass surface density maps (down to $10^{5}M_{\odot}\,\mathrm{kpc}^{-2}$, where $M_{\odot}$ is the mass of the Sun). The clear presence of these galaxies in the stellar images and absence in the dark matter maps is remarkable. To illustrate, the right-hand panels display two special cases: Bird and Long Hair, the members with the most and least active interaction histories in our set of seven.

[1]Department of Physics and Astronomy, Pomona College, Claremont, CA, USA. [2]Department of Physics and Astronomy, University of California, Irvine, CA, USA. [3]TAPIR, California Institute of Technology, Pasadena, CA, USA. [4]Department of Astrophysical Sciences, Princeton University, Princeton, NJ, USA. [5]Institute for Advanced Study, Princeton, NJ, USA. [6]Institute for Computational Science, University of Zurich, Zurich, Switzerland. [7]Department of Physics & Astronomy and CIERA, Northwestern University, Evanston, IL, USA. [8]Carnegie Observatories, Pasadena, CA, USA. [9]Department of Physics and Astronomy, California State Polytechnic University, Pomona, Pomona, CA, USA. [10]Department of Physics & Astronomy, University of California, Davis, Davis, CA, USA. [11]Department of Physics, University of Connecticut, Storrs, CT, USA. [12]Center for Computational Astrophysics, Flatiron Institute, New York, NY, USA. [13]Department of Astronomy, University of Texas at Austin, Austin, TX, USA. [14]Department of Physics, Center for Astrophysics and Space Sciences, University of California San Diego, La Jolla, CA, USA. ✉e-mail: jorge.moreno@pomona.edu

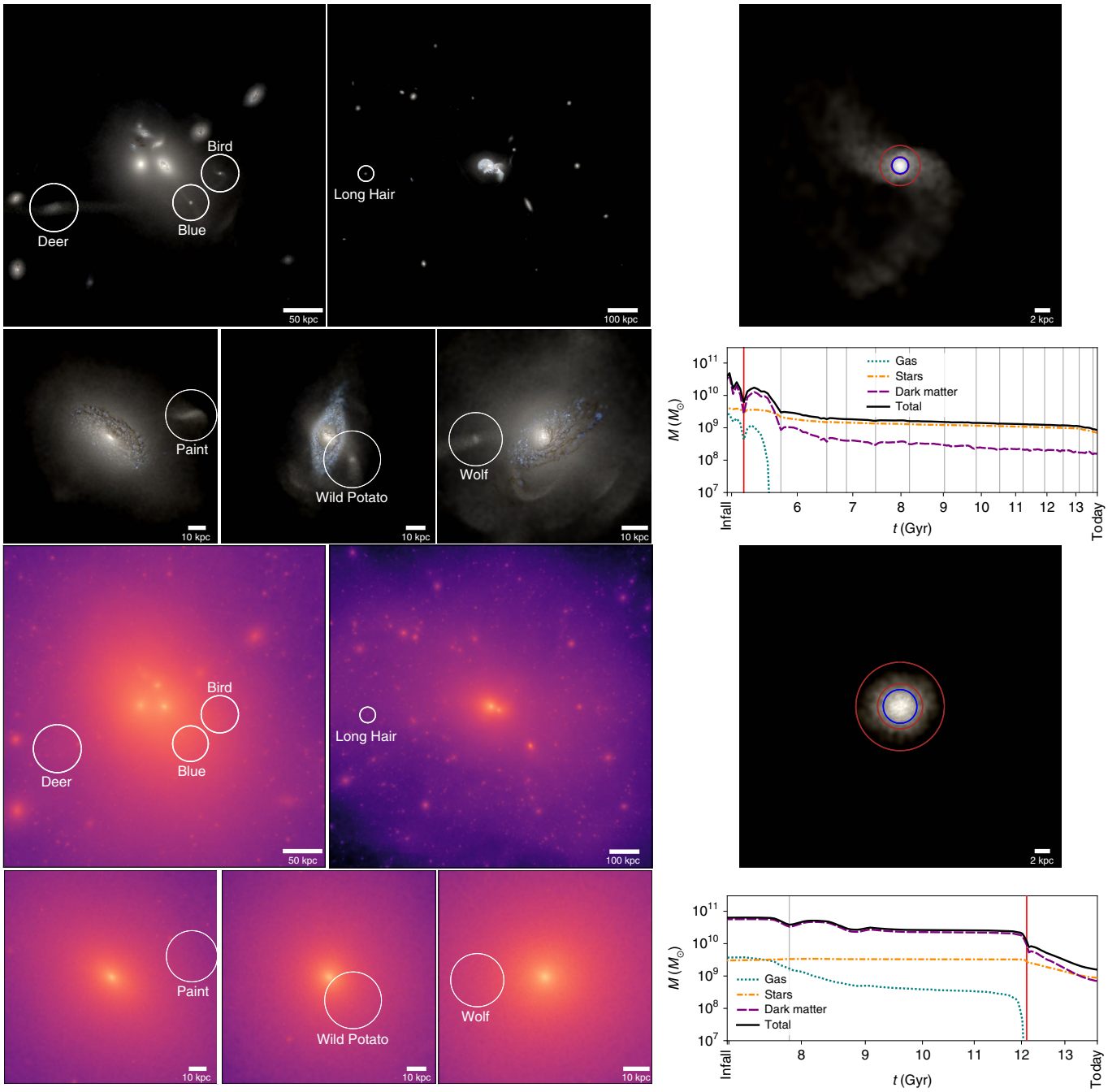

Fig. 1 | Galaxies lacking dark matter. Top left: mock stellar Hubble Space Telescope u/g/r composite images of the environments around our seven dark-matter-deficient galaxies at the present time ($z=0$) with a cut-off of 28.9 mag arcsec^{-2} (corresponding to $10^5\,L_\odot$ kpc^{-2}). Bottom left: dark-matter-mass surface density maps (down to $10^5 M_\odot$ kpc^{-2}). The satellites are clearly visible in the stellar images but not in the dark matter maps. Right: magnified mock stellar images (top) and masses inside the subhalo radius versus time (t, bottom) of Bird (top) and Long Hair (bottom). The red circles indicate the radii containing 50 and 80% of the stellar mass, and the blue circle refers to the effective radius in the g-band. The grey vertical lines mark pericentric passages, red vertical lines mark the closest pericentric passage.

At the present time (redshift $z=0$), Bird, Blue and Deer inhabit the same galaxy group (virial mass $M_{\rm vir}=1.8\times10^{13}\,M_\odot$) and are at 80 kpc, 66 kpc and 174 kpc away from its centre, respectively. Long Hair also lives in a group ($M_{\rm vir}=1.4\times10^{13}\,M_\odot$) and has the largest halocentric distance (484 kpc) amongst the seven. Paint, Wild Potato and Wolf exist in haloes slightly more massive than that of the Milky Way ($M_{\rm vir}=3.6$, 2.5 and $3.3\times10^{12}\,M_\odot$) and have halocentric distances of 72 kpc, 57 kpc and 36 kpc. The two observed galaxies lacking dark matter, DF2 (ref. [6]) and DF4 (ref. [7]) are at close projected separations (80 kpc and 165 kpc, which set a lower limit to the 3D separations) from NGC 1052[31,32] (stellar mass $M_\star=1.05\times10^{11}\,M_\odot$; ref. [33]). Following ref. [34], we estimate that NGC 1052 has $M_{\rm vir}=6.2^{+25.8}_{-4.2}\times10^{12}M_\odot$ at 90% confidence, which is consistent with the $M_{\rm vir}$ of our hosts. Although halocentric separations vary with time, their present-day values can provide information about their current membership status as satellites (see below).

Figure 2 shows dark matter mass ($M_{\rm dm}$) versus $M_\star$. Hereafter, we report quantities within $r_{50}^\star$, the radius containing 50% of the stellar

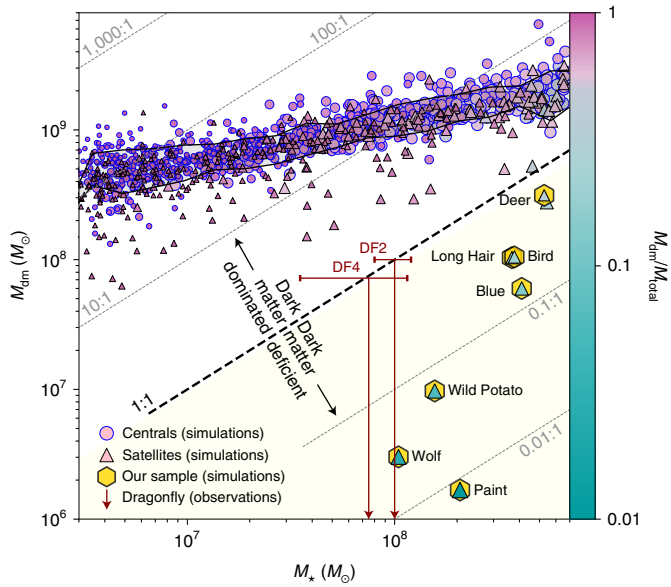

Fig. 2 | Fraction of mass in dark matter in simulated and observed galaxies. Dark matter mass versus stellar mass, colour coded by the fraction of the total mass in dark matter (M_{dm}/M_{total}). Masses are determined within $r_{50}^\star$. Symbol dimensions scale inversely with M_{dm}/M_{total}. The light grey band bounded by black lines represents the median and standard deviation (simulated centrals only). The light yellow region denotes the dark-matter-deficient regime. The yellow hexagons highlight our sample of simulated galaxies lacking dark matter. The red arrows with error bars (1 s.d.) represent observations[6,7] conducted with the Dragonfly Telephoto Array.

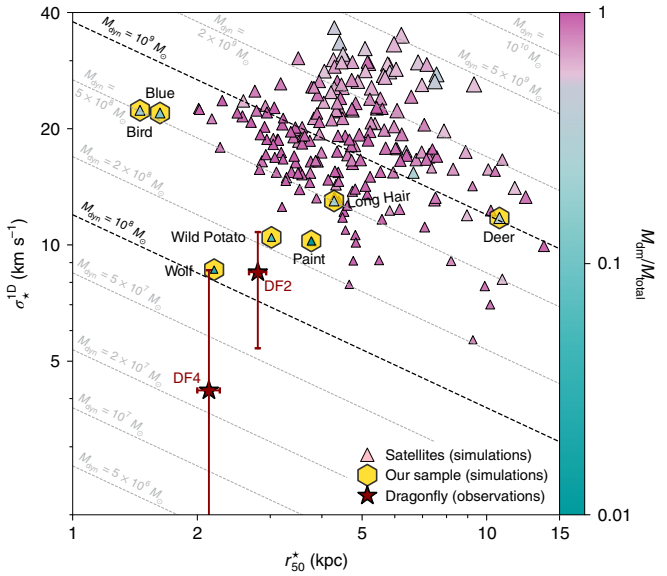

Fig. 3 | Comparison of internal properties in simulated and observed galaxies. Quantities are measured within $r_{50}^\star$. The triangles denote simulated satellites with $M_\star = 10^{8\text{–}9}\,M_\odot$, their dimensions scale with M_{total} and are colour coded by M_{dm}/M_{total}. The red stars with error bars (1 s.d.) represent Dragonfly observations[7,35]. The diagonal dashed lines show various fixed dynamical masses according to an analytic mass estimator[39]: $M_{dyn}(< r_{50}^\star) \propto (\sigma_\star^{1D})^2\, r_{50}^\star$.

mass, to compare directly with observations[35] (red arrows with error bars). We note, however, that our seven galaxies are also dark-matter deficient out to larger galactocentric radii (Supplementary Table 2 and Supplementary Fig. 9). The diagonal lines represent constant dark-matter-to-stellar mass ratios. We selected our sample of seven dark-matter-deficient galaxies (yellow hexagons) by requiring $M_{dm} < M_\star$ (light yellow region below the 1:1 line). Wolf's stellar mass is consistent with both DF2 and DF4. We did not include galaxies with $M_\star < M_{dm} < M_{baryon}$, where M_{baryon} is the baryonic mass, in this sample. These are probably simulated analogues of the recently discovered baryon-rich galaxies[36–38], which we plan to study separately. (We also discarded one object, the triangle in close proximity to Deer, because it is participating in an ongoing gas-rich merger, unlike DF2 and DF4.)

Figure 3 shows the one-dimensional (1D) line-of-sight velocity dispersion ($\sigma_\star^{1D}$) versus the galactic size ($r_{50}^\star$). For observations of DF2 and DF4, we used deprojected measurements[39] from ref. [35] and ref. [7], respectively. For comparison, we also included simulated galaxies with $M_\star = 10^{8\text{–}9}\,M_\odot$ (within $r_{50}^\star$), in line with our sample of seven. We note that although this stellar-mass regime contains DF2 and DF4, it is 'too generous'. Specifically, only galaxies with $M_\star$ (within $r_{50}^\star$) close to $10^8\,M_\odot$ may qualify as realistic numerical analogues of DF2 and DF4 (the rest should thus be regarded as slightly more massive predictions). To guide the eye, the dashed diagonal lines track fixed dynamical masses within $r_{50}^\star$ according to an analytic mass estimator[39]. To quantify the morphology of our seven galaxies, we also performed Sérsic[40] profile fittings in the g-band. We measured effective 2D radii (R_e^{2D}), which are in line with our $r_{50}^\star$ values after deprojection (Supplementary Figs. 2 and 3 and Supplementary Table 1). With this procedure, we also obtained Sérsic indices ($n_{Sérsic}$), which range from 0.60–0.77, in excellent agreement with observations ($n_{Sérsic} = 0.60$ and 0.79 for DF2 and DF4, respectively).

Our results thus far suggest that Wolf is the only dark-matter-deficient galaxy in the cosmological simulation literature that simultaneously matches observations on the following fronts: stellar mass (within $r_{50}^\star$), $\sigma_\star^{1D}$, size and morphology (Wild Potato has $\sigma_\star^{1D} = 7.0\,\mathrm{km\,s^{-1}}$ along one of the three orthogonal directions we report, but is has marginally higher stellar mass than DF2 and DF4; Supplementary Fig. 4 and Supplementary Table 1).

Previous cosmological simulations have not been able to match the aforementioned internal properties of the two observed dark-matter-deficient galaxies. The most promising object in ref. [17] has ~66% more mass in dark matter relative to stars, whereas the stellar mass and $\sigma_\star^{1D}$ in the simulations reported by ref. [10] exceed observational measurements by more than 1 s.d. See Supplementary Fig. 9 for a direct comparison with those two works. Furthermore, other cosmological simulations have been unable to produce low-mass galaxies with dark-matter mass fractions as low as ours: three members of our sample have dark-matter mass fractions below 10% and one has only 1% of its mass in dark matter—rendering them almost dark-matter-free galaxies. One possible explanation is that our simulation has the distinct advantage of being able to model the small-scale (~20 pc) interstellar medium and the high densities (>300 cm^{-3}) of star-forming gas of individual galaxies within a cosmological region (~20 Mpc on a side) large enough to contain several massive groups of galaxies. See Supplementary Fig. 9 and the associated text for a detailed comparison with results from other groups.

Below we show that close encounters are responsible for the creation of dark-matter-deficient galaxies in our simulation. Observationally, it is challenging to infer whether a galaxy has experienced close interactions in its history. For instance, Bird exhibits 'S-shaped' low-surface-brightness tails, whereas Long Hair seems to be undisturbed (see magnified examples on the right-hand side of Fig. 1 and Supplementary Fig. 5 for a more detailed analysis of Long Hair). However, our simulation reveals that close encounters with a massive neighbour are responsible for dark-matter deficiency in all

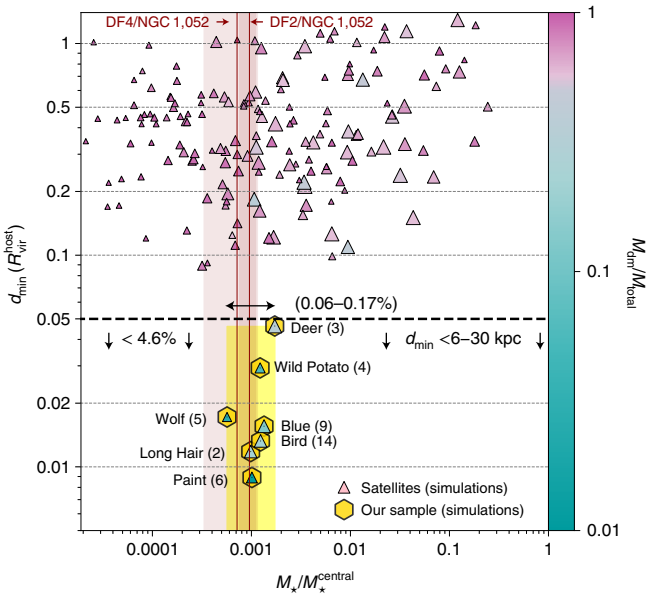

Fig. 4 | Conditions for creating a galaxy lacking dark matter. d_{min} versus $M_\star/M_\star^{central}$. The triangles denote simulated satellites with $M_\star = 10^{8\text{–}9}\,M_\odot$, colour coded by M_{dm}/M_{total}, with dimensions scaled by $M_\star$ (simulations). Quantities are within $r_{50}^\star$ for satellites and $r_{80}^\star$ for centrals. The yellow rectangle, percentages within parentheses and values between downward arrows highlight the region of the parameter space that our seven galaxies occupy (yellow hexagons) and the numbers in parentheses indicate number of pericentric passages. The vertical red lines (and bands) denote the stellar mass ratios (and uncertainty) between DF2/DF4 and NGC 1052 (observations).

of our seven galaxies. They all started out more massive, gas rich and with fairly typical stellar-to-dark-matter mass ratios for galaxies of their mass, but subsequently experienced multiple close interactions with their host galaxies (see the mass-evolution insets in Fig. 1 and Supplementary Fig. 7). With the exception of Deer, these galaxies lost all of their gas during this process, in agreement with DF2[41]. These satellites also lost between 97.9 and 99.99% of their dark matter mass whilst losing only 45–97% of their stellar mass (within the subhalo radius); see Supplementary Table 2 and Supplementary Fig. 8 for details). We suspect that stars are more resilient, as they move on more circular orbits than the eccentric orbits of the dark matter particles. Differences in the elongation and dynamical times of the orbits followed by dark matter particles relative to those followed by stars thus leave them more susceptible to tidal stripping[42–45].

To quantify the role of interactions, we evaluated how close satellite galaxies came to their hosts and their stellar mass ratios relative to those massive central companions. Figure 4 shows d_{min}, the minimum halocentric distance ever attained by each satellite (given in units of R_{vir}^{host}, the final virial radius of the host) versus $M_\star/M_\star^{central}$, the present-day satellite–central stellar mass ratio. For satellites, we continued to employ $r_{50}^\star$, whereas for centrals, we switched to $r_{80}^\star$, which better captures their spatial extent[46]. Our simulation suggests that, to become a dark-matter-deficient galaxy, a satellite must pierce within ~5% (below horizontal black dashed line) of the host virial radius (within ~6–30 kpc, depending on the host). In other words, the satellite must transit through the host's stellar body. We also predict that their satellite–central stellar-mass ratio must be ~0.1%. The yellow region in Fig. 4 indicates these two conditions. The stellar mass ratios of DF2 and DF4 relative to NGC 1052 are consistent with our simulation; however, no orbital information is available to determine d_{min}.

Whether or not the galaxies in our simulation formed in the same way as DF2 and DF4 is still unclear. Our results support a scenario where DF2 and DF4 became dark-matter deficient due to past close encounters with NGC 1052, the only massive galaxy in their neighbourhood (note that our simulation allowed hosts to have multiple dark-matter-deficient satellites). Their projected (80 kpc and 165 kpc) and line-of-sight separations (2.1 ± 0.5 Mpc)[31]—as well as our estimates of the virial diameter of the NGC 1052 halo—suggest that DF2 and DF4 could be satellites of the NGC 1052 group. Using ref. [34], we estimated this galaxy group to have a virial diameter of 0.7–1.7 Mpc at 90% confidence, allowing for the possibility that NGC 1052 could encompass both objects. This possibility increases if either DF2 or DF4 are a 'backsplash'[47] galaxy; that is, a galaxy on an extremely radial orbit that carried it beyond the virial volume of NGC 1052 after a close encounter (we note that our simulated sample includes two recent backsplash galaxies: Long Hair and Deer). Future efforts to determine accurate 3D separations between DF2 and DF4 relative to NGC 1052 will provide an important test of this interaction-based scenario.

Although we have successfully created a galaxy (Wolf) in a cosmological simulation that matches DF2 and DF4 remarkably well (in terms of $M_\star$, $r_{50}^\star$, $\sigma_\star^{1D}$ and $n_{Sérsic}$), a few issues remain. In addition to being dark-matter deficient, DF2 and DF4 are intriguing because they (1) inhabit the same group and (2) are extremely similar to each other. Namely, they resemble each other in terms of stellar mass, size, (extremely low) velocity dispersion, Sérsic index, colour and the presence of anomalous globular cluster populations[48]. Our cosmological simulation has insufficient resolution to explore the globular cluster problem, but zoom-in simulations with our model could address this[49,50]. However, we were able to measure stellar population properties in our seven dark-matter-deficient galaxies (Supplementary Table 3). In particular, Blue and Bird have stellar ages of 10 and 8.7 Gyr, in line with DF2[6] (8.9 ± 1.5 Gyr). Indeed, just like DF2 and DF4, these two simulated galaxies also inhabit the same group (Fig. 1). However, despite having some of the lowest metallicities in our set of seven ($\langle$[Fe/H]$\rangle = -0.61$ and -0.34), they are not as metal poor as DF2[51] ($\langle$[Fe/H]$\rangle = -1.35 \pm 0.12$). One possibility is that DF2 and DF4 had infall stellar masses similar to Blue and Bird, but sat initially on the lower envelope of their mass–metallicity relation. Confirming the existence of such objects would require a larger simulation box or multiple distinct realizations of this simulation (with the same physics but different initial conditions).

In summary, our results demonstrate that galaxies resembling DF2 and DF4 can arise naturally within the standard cold dark matter cosmological paradigm. We note that we did not expect this to occur a priori (that is, our simulation was not originally designed for this purpose). Although there certainly is still room for new physics beyond the standard paradigm, discriminating between alternative models will now rely on predicted differences between the expected properties of dark-matter-deficient galaxies, rather than their mere existence[8].

To efficiently uncover more galaxies devoid of dark matter, we recommend that observers focus on satellites with $M_\star = 10^{8\text{–}9}\,M_\odot$ near massive companions ($M_\star \geq 10^{11}\,M_\odot$). We predict that 30% of such massive galaxies will have at least one dark-matter-deficient satellite. We also predict that only 30% of haloes with viral masses $\geq 2 \times 10^{12}$ (the lower bound for NGC 1052;) will harbour such peculiar objects. This mass range is slightly above the virial masses of the Milky Way and Andromeda—which might explain why no analogues of DF2 and DF4 have been detected in the Local Group. However, we cannot exclude a situation in which a central–satellite pair outside this mass regime could have a sufficiently unorthodox orbital configuration to produce the same effect. Verifying how strict this regime is will require a larger volume (or more realisations). More generally, to truly constrain the varied processes

and underlying physics governing these galaxies, ambitious observational campaigns aiming to enumerate and characterise large samples of galaxies with unusual dark-matter properties will be desirable in the years ahead.

Methods

Our cosmological simulation. We ran a high-resolution cosmological simulation of galaxy formation with box size of 21 comoving Mpc and the following number of baryonic and dark matter particles: $N_{\rm baryon}=1,024^3$ and $N_{\rm dm}=1,024^3$. Initially, the baryonic particle masses were $m_{\rm baryon}=6.3\times10^4\,M_\odot$ for gas and star particles, whereas the dark matter particles had $m_{\rm dm}=3.3\times10^5\,M_\odot$. The force resolution was set at a fixed $h_{\rm star}=12$ pc (physical) for star particles and 80 pc for dark matter particles. For gas, the force resolution was set equal to the adaptive smoothing length down to a minimum of 1.5 pc, which occurred only in the densest regions of galaxies. We identified galaxies (and merger history trees) with the AMIGA Halo Finder (AHF[52]), which uses an iterative unbinding procedure to identify gravitationally bound objects[53]. This method assumes the virial-mass definition of ref. [54] by construction. We used yt[55] to interface with the particle data. The cosmological parameters were set to $\Omega_{\rm matter}=0.3089$ (matter contribution to the critical density), $\Omega_\Lambda=0.6911$ (cosmological contribution to the critical density), $\Omega_{\rm baryon}=0.0486$ (baryonic contribution to the critical density), $\sigma_8=0.8159$ (amplitude of the linear power spectrum at scales of 8 h^{-1} Mpc and $h=0.6774$ (scaled Hubble constant).

We employed the FIRE-2 model[24] for baryonic physics, which includes radiative cooling and star formation in dense self-gravitating gas, and accounts for stellar feedback in the form of supernovae, stellar mass-loss and radiation interacting with the surrounding gas (as described therein). We followed 11 separately tracked species: H, He, C, N, O, Ne, Mg, Si, S, Ca and F. This model has been extensively validated in a number of publications analysing the properties of galaxies across a range of stellar masses and numerical resolutions[25]. In our run, star formation occurred only in gas denser than $n=300\,{\rm cm}^{-3}$. Under this condition, the interparticle separation in star-forming gas was ~20 pc (or less) and we were able to resolve giant-molecular-cloud complexes within the interstellar medium of individual galaxies.

Our simulated galaxy samples. In this work we focused on galaxies with at least 100 stellar particles at $z=0$. The actual number of particles per object is typically much larger owing to an additional contribution of gas and dark matter particles for each object, either at the present time or at some point in its history. To avoid discarding galaxies lacking dark matter, our application of AHF used all types of particle, not just dark matter. This came at a price: the halo finder falsely identified large numbers of gas clumps within galaxies as individual 'galactic units'. To address this, we first discarded objects with baryon-to-total mass ratios greater than 0.5. This may naturally discard the very objects we sought (and keep false clumps below this threshold). To ameliorate this, we created surface density maps of every halo with substructures and visually recovered objects that might have been discarded erroneously by our 50% cut. The images shown in Fig. 1 belong to this set. We focused on manually deleting clumps embedded inside massive galaxies and on recovering galaxies that are either clearly disjoint from their neighbours or in tidal tails, to avoid rejecting tidally formed candidates[56]. We highlight that every galaxy lacking dark matter studied in this paper was recovered during this step. Lastly, because we were interested in the low-mass regime, we constrained our sample to have stellar masses under $10^9\,M_\odot$ (within $r^\star_{80}$, the radius containing 80% of the stellar mass). This produced our final parent sample, which contained 1,218 resolved galaxies: 886 centrals and 332 satellites. See Supplementary Fig. 1 for a visual description of these two sets.

Our dark-matter-deficient set consisted of seven galaxies with $M_{\rm dm}<M_\star$ that are not participating in a major merger (we discarded an eighth galaxy meeting the former condition, but not the latter). We adopted this extra condition because the two observed Dragonfly galaxies are not currently merging with a companion of similar mass. We also exclude 19 low-mass galaxies (15 centrals and 4 satellites) with $M_{\rm dm}<M_{\rm baryon}$ (but $M_{\rm dm}>M_\star$) that are possibly numerical analogues of the recently observed baryon-rich galaxies[36–38]. The final set of seven comprised satellites with $M_\star=10^{8\text{–}9}\,M_\odot$; they orbit five different massive central galaxies with $M_\star>10^{11}\,M_\odot$. In total, our simulation contained 15 massive centrals that host 47 satellite galaxies in the target stellar mass range ($10^{8\text{–}9}\,M_\odot$). Of these satellites, ~15% belong to our set of seven, which orbit ~30% of the available massive centrals.

The absence of dark-matter-deficient satellite galaxies at stellar masses below $10^8\,M_\odot$ could arise from the fact that, at lower masses, galaxies are born as centrals with very high dark matter mass fractions, such that environmental effects cannot act to remove dark matter without completely destroying the galaxy. The absence of dark-matter-deficient galaxies at lower stellar masses is probably not driven by a lack of resolution, because our simulation produced a large population of galaxies with at least 1,000 stellar particles that are less massive than Wolf (which has 3,280 stellar particles at $z=0$ and had a factor of ~35 higher before becoming a satellite). For a discussion about potential numerical effects on tidal disruption, see Supplementary Fig. 8 and the associated text.

Galactic sizes. We calculated galactic sizes as follows. For each object, we recorded the distance to the nearest major companion (with a stellar mass of at least a tenth of that of our object of interest). If no such companion existed, we recorded the virial radius (for centrals) or subhalo radius (for satellites). This step was necessary because AHF considers substructures as part of their host. Once this region was identified, we calculated the stellar centre of mass. Next we redefined the radius of this region by subtracting the distance from the origin to this centre of mass. Within this region, we then calculated cumulative mass profiles (using 200 identical linear radial bins) and extracted the radius containing 80% of the stellar mass within this region by linearly interpolating between the two radii below and above this threshold. The sizes of our seven dark-matter-deficient galaxies are listed in Supplementary Table 1 and displayed in Supplementary Figs. 2 and 3.

$\sigma^{\rm 1D}_\star$. We also calculated $\sigma^{\rm 1D}_\star$ within $r^\star_{50}$. We performed this calculation along three random directions (in the frame of each galaxy), corresponding to the x, y and z directions in the frame of the box. We created histograms of line-of-sight velocity minus the average line-of-sight velocity within $r^\star_{50}$. These histograms have bin widths of 2 km s^{-1} and extend from −70 to 70 km s^{-1}. We then fitted a Gaussian curve and recorded its σ value. In the main text we reported the simple average of these three numbers. The $\sigma^{\rm 1D}_\star$ values for our seven dark-matter-deficient galaxies are listed Supplementary Table 1 and displayed (along the aforementioned three directions) in Supplementary Fig. 4

Data availability

The datasets generated during and/or analysed during the current study are available from the corresponding author on reasonable request, contingent on approval by the FIRE Collaboration on a case-by-case basis.

Code availability

The codes we used are available as follows: GIZMO, https://bitbucket.org/phopkins/gizmo-public/src/master; yt, https://yt-project.org; AHF, http://popia.ft.uam.es/AHF/Download.html; FIRE Studio, https://github.com/agurvich/FIRE_studio; WebPlotDigitizer, https://apps.automeris.io/wpd.The Python scripts used to create the Figs. 1–4 and Supplementary Figs. 1–9 are available from the corresponding author on reasonable request, contingent on approval by the FIRE Collaboration on a case-by-case basis.

Received: 17 November 2021; Accepted: 20 December 2021;
Published online: 14 February 2022

References

1. Zwicky, E. Die rotverschiebung von extragalaktischen nebeln. *Helv. Phys. Acta* **6**, 110–127 (1933).
2. Rubin, B. C. & Ford, W. K. Jr Rotation of the Andromeda Nebula from a spectroscopic survey of emission regions. *Astrophys. J.* **159**, 379 (1970).
3. White, S. D. M. & Rees, M. J. Core condensation in heavy halos: a two-stage theory for galaxy formation and clustering. *Mon. Not. R. Astron. Soc.* **183**, 341–358 (1978).
4. Behroozi, P. S., Wechsler, R. H. & Conroy, C. The average star formation histories of galaxies in dark matter halos from z=0-8. *Astrophys. J.* **770**, 57 (2013).
5. Tollerud, E. et al. From galaxy clusters to ultra-faint dwarf spheroidals: a fundamental curve connecting dispersion-supported galaxies to their dark matter halos. *Astrophys. J.* **726**, 23 (2011).
6. van Dokkum, P. et al. A galaxy lacking dark matter. *Nature* **555**, 629–632 (2018).
7. van Dokkum, P. et al. A second galaxy missing dark matter in the NGC 1052 group. *Astrophys. J. Lett.* **874**, 1 (2019).
8. Haslbauer, M., Banik, I., Kroupa, P. & Grishunin, K. The ultra-diffuse dwarf galaxies NGC 1052-DF2 and 1052-DF4 are in conflict with standard cosmology. *Mon. Not. R. Astron. Soc.* **489**, 2634–2651 (2019).
9. Yu, H., Ratra, B. & Wang, F.-J. Dark matter deficient galaxies in the Illustris flat-Λ CDM model structure formation simulation. Preprint at https://arxiv.org/abs/1809.05938 (2018).
10. Jing, Y. et al. Dark-matter-deficient galaxies in hydrodynamical simulations. *Mon. Not. R. Astron. Soc.* **488**, 3298–3307 (2009).
11. Haslbauer, M. et al. Galaxies lacking dark matter in the Illustris simulation. *Astron. Astrophys.* **626**, A47 (2019).
12. Carleton, T. et al. The formation of ultra diffuse galaxies in cored dark matter haloes through tidal stripping and heating. *Mon. Not. R. Astron. Soc.* **485**, 382–395 (2019).
13. Sales, L. V. et al. The formation of ultradiffuse galaxies in clusters. *Mon. Not. R. Astron. Soc.* **494**, 1848–1858 (2020).
14. Saulder, C. et al. Isolated dark-matter-deprived galaxies in hydrodynamical simulations: real objects or artifacts? *Mon. Not. R. Astron. Soc.* **491**, 1278–1286 (2020).

15. Shin, E. et al. Dark matter deficient galaxies produced via high-velocity galaxy collisions in high-resolution numerical simulations. *Astrophys. J.* **899**, 25 (2020).
16. Applebaum, E. et al. Ultrafaint dwarfs in a Milky Way context: introducing the Mint condition DC Justice League simulations. *Astrophys. J.* **909**, 96 (2021).
17. Jackson, R. A. et al. Dark matter-deficient dwarf galaxies form via tidal stripping of dark matter in interactions with massive companions. *Mon. Not. R. Astron. Soc.* **502**, 1785–1796 (2021).
18. Wright, A. C. The formation of isolated ultradiffuse galaxies in ROMULUS25. *Mon. Not. R. Astron. Soc.* **502**, 5370–5389 (2021).
19. Ogiya, G. Tidal stripping as a possible origin of the ultra diffuse galaxy lacking dark matter. *Mon. Not. R. Astron. Soc.* **480**, L106–L110 (2018).
20. Huo, R. Refracting into ultra-diffuse galaxy NGC 1052-DF2 by passing near the centre of NGC 1052. *Mon. Not. R. Astron. Soc.* **495**, L144–L148 (2020).
21. Nusser, A. A scenario for ultradiffuse satellite galaxies with low velocity dispersions: the case of [KKS 2000]04. *Astrophys. J.* **893**, 66 (2020).
22. Yang, D., Yu, H.-B. & An, H. Self-interacting dark matter and the origin of ultradiffuse galaxies NGC1052-DF2 and -DF4. *Phys. Rev. Lett.* **125**, 111105 (2020).
23. Macciò, A. V. et al. Creating a galaxy lacking dark matter in a dark matter-dominated universe. *Mon. Not. R. Astron. Soc.* **501**, 693–700 (2021).
24. Hopkins, P. F. et al. FIRE-2 simulations: physics versus numerics in galaxy formation. *Mon. Not. R. Astron. Soc.* **480**, 800–863 (2018).
25. Faucher-Giguére, C.-A. Recent progress in simulating galaxy formation from the largest to the smallest scales. *Nat. Astron.* **2**, 368–373 (2018).
26. Kroupa, P. et al. Does the galaxy NGC1052-DF2 falsify Milgromian dynamics?. *Nature* **561**, E4–E5 (2018).
27. Moffat, J. W. & Toth, V. T. NGC 1052-DF2 and modified gravity (MOG) without dark matter. *Mon. Not. R. Astron. Soc.* **482**, L1–L3 (2019).
28. Khalifeh, A. R. & Jimenez, R. Dwarf galaxies without dark matter: constraints on modified gravity. *Mon. Not. R. Astron. Soc.* **501**, 254–260 (2021).
29. Famaey, B., McGaugh, S. & Milgrom, M. MOND and the dynamics of NGC 1052-DF2. *Mon. Not. R. Astron. Soc.* **480**, 473–476 (2018).
30. Haghi, H. et al. A new formulation of the external field effect in MOND and numerical simulations of ultra-diffuse dwarf galaxies – application to NGC 1052-DF2 and NGC 1052-DF4. *Mon. Not. R. Astron. Soc.* **487**, 2442–2454 (2019).
31. Shen, Z. et al. A tip of the red giant branch distance of 22.1 ± 1.2 Mpc to the dark matter deficient galaxy NGC 1052-DF2 from 40 orbits of Hubble Space Telescope imaging. *Astrophys. J. Lett.* **914**, L12 (2021).
32. Danieli, S. et al. A tip of the red giant branch distance to the dark matter deficient galaxy NGC 1052-DF4 from Deep Hubble Space Telescope data. *Astrophys. J. Lett.* **895**, L4 (2020).
33. Forbes, D. A. et al. The SLUGGS Survey: stellar masses and effective radii of early-type galaxies from Spitzer Space Telescope 3.6 μm imaging. *Mon. Not. R. Astron. Soc.* **464**, 4611–4623 (2017).
34. Zahid, H. J., Sohn, J. & Geller, M. J. Stellar velocity dispersion: linking quiescent galaxies to their dark matter haloes. *Astrophys. J.* **859**, 96 (2018).
35. Danieli, S. et al. Still missing dark matter: KCWI high-resolution stellar kinematics of NGC1052-DF2. *Astrophys. J. Lett.* **874**, L12 (2019).
36. Mancera Piña, P. et al. Off the baryonic Tully-Fisher relation: a population of baryon-dominated ultra-diffuse galaxies. *Astrophys. J.* **883**, L33 (2019).
37. Guo, Q. et al. Further evidence for a population of dark-matter-deficient dwarf galaxies. *Nat. Astron.* **4**, 246–251 (2020).
38. Mancera Piña, P. et al. No need for dark matter: resolved kinematics of the ultra-diffuse galaxy AGC 114905. Preprint at https://arxiv.org/abs/2112.00017 (2021).
39. Wolf, J. et al. Accurate masses for dispersion-supported galaxies. *Mon. Not. R. Astron. Soc.* **406**, 1220–1237 (2010).
40. Sérsic, J. L. Influence of the atmospheric and instrumental dispersion on the brightness distribution in a galaxy. *Bol. Asoc.Argent. Astron.* **6**, 41–43 (1963).
41. Sardone, A. et al. Constraints on the HI mass of NGC 1052-DF2. *Astrophys. J.* **871**, 31 (2019).
42. Peñarrubia, J. et al. The impact of dark matter cusps and cores on the satellite galaxy population around spiral galaxies. *Mon. Not. R. Astron. Soc.* **406**, 1290–1305 (2010).
43. Bryan, S. E. Influence of baryons on the orbital structure of dark matter haloes. *Mon. Not. R. Astron. Soc.* **422**, 1863–1879 (2013).
44. Valluri, M. et al. Probing the shape and history of the Milky Way halo with orbital spectral analysis. *Mon. Not. R. Astron. Soc.* **419**, 1951–1969 (2013).
45. Zhu, Q. et al. Baryonic impact on the dark matter orbital properties of Milky Way-sized haloes. *Mon. Not. R. Astron. Soc.* **466**, 3876–3886 (2017).
46. Mowla, L., van der Wel, A., van Dokkum, P. & Miller, T. B. A mass-dependent slope of the galaxy size-mass relation out to $z \sim 3$: further evidence for a direct relation between median galaxy size and median halo mass. *Astrophys. J. Lett.* **872**, L13 (2019).
47. Wetzel, A. R. et al. Galaxy evolution near groups and clusters: ejected satellites and the spatial extent of environmental quenching. *Mon. Not. R. Astron. Soc.* **439**, 2687–2700 (2014).
48. Shen, Z. et al. A complex luminosity function for the anomalous globular clusters in NGC 1052-DF2 and NGC 1052-DF4. *Astrophys. J.* **909**, 179 (2021).
49. Kim, J. H. et al. Formation of globular cluster candidates in merging proto-galaxies at high redshift: a view from the FIRE cosmological simulations. *Mon. Not. R. Astron. Soc.* **474**, 4232–4244 (2018).
50. Ma, X. et al. Self-consistent proto-globular cluster formation in cosmological simulations of high-redshift galaxies. *Mon. Not. R. Astron. Soc.* **493**, 4315–4332 (2020).
51. Fensch, J. et al. The ultra-diffuse galaxy NGC 1052-DF2 with MUSE II. The population of DF2: stars, clusters, and planetary nebulae. *Astron. Astrophys.* **625**, A77 (2019).
52. Knollmann, S. R. & Knebe, A. AHF: AMIGA's Halo Finder. *Astrophys. J. Suppl. Ser.* **182**, 608–624 (2009).
53. Knebe, A. et al. Haloes gone MAD: the Halo-Finder Comparison Project. *Mon. Not. R. Astron. Soc.* **415**, 2293–2318 (2011).
54. Bryan, G. L. & Norman, M. L. Statistical properties of X-ray clusters: analytic and numerical comparisons. *Astrophys. J.* **495**, 80 (1998).
55. Turk, M. J. et al. yt: a multi-code analysis toolkit for astrophysical simulation data. *Astrophys. J. Suppl. Ser.* **192**, 96 (2011).
56. Elmegreen, B. G., Kaufman, M. & Thomasson, M. An interaction model for the formation of dwarf galaxies and 10^8 Msun clouds in Spiral Disks. *Astrophys. J.* **412**, 90 (1993).

Acknowledgements

Sabbatical leave support from Pomona College and the Harry and Grace Steele Foundation (J.M.). NASA Hubble Fellowship grant number HST-HF2-51454.001-A awarded by the Space Telescope Science Institute, which is operated by the Association of Universities for Research in Astronomy, Incorporated, under NASA contract number NAS5-26555 (S.D.). NSF grant number AST-1910346 (J.S.B., F.J.M. and S.Y.). Swiss National Science Foundation grant numbers PP00P2_157591, PP00P2_194814 and 200021_188552; Swiss National Supercomputing (CSCS) project IDs s697 and s698 (R.F.). NSF Research Grant numbers 1911233 and 20009234, NSF CAREER grant number 1455342, NASA grant numbers 80NSSC18K0562 and HST-AR-15800.001-A (P.F.H.). NASA grant number 80NSSSC20K1469 (A.L.). Gary McCue postdoctoral fellowship through the Center for Cosmology at UC Irvine (Z.H.). National Science Foundation Graduate Research Fellowship under grant number DGE-1839285 (C.K.). NSF CAREER grant number 2045928; NASA ATP grant numbers 80NSSC18K1097 and 80NSSC20K0513; HST grant numbers AR-15809 and GO-15902 from STScI; Scialog Award from the Heising-Simons Foundation; Hellman Fellowship (A.W.). NSF grant number AST-2009687 and by the Flatiron Institute, which is supported by the Simons Foundation (D.A.-A.). NSF CAREER award number AST-1752913, NSF grant number AST-1910346, NASA grant numbers NNX17AG29G and HST-AR-15006, HST-AR-15809, HST-GO-15658, HST-GO-15901, HST-GO-15902, HST-AR-16159 and HST-GO-16226 from STScI (M.B.-K.). Simons Investigator Award from the Simons Foundation; NSF grant number AST-1715070 (E.Q.). NSF through grant numbers AST-1715216 and CAREER award AST-1652522; by NASA through grant number 17-ATP17-0067; by STScI through grant number HST-AR-16124.001-A; and by the Research Corporation for Science Advancement through a Cottrell Scholar Award and a Scialog Award (C.-A.F.-G.). NSF grant number AST-1715101 (D.K.). Numerical calculations were run on the Caltech compute cluster "Wheeler," allocations FTA-HopkinsAST20016 supported by the NSF and TACC and NASA HEC SMD-16-7592. We acknowledge PRACE for awarding us access to MareNostrum at the Barcelona Supercomputing Center (BSC), Spain. This research was partly carried out via the Frontera computing project at the Texas Advanced Computing Center. Frontera is made possible by National Science Foundation award number OAC-1818253. We acknowledge access to Piz Daint at the Swiss National Supercomputing Centre, Switzerland under the University of Zurich's share with the project ID uzh18. Additional computing support was provided by S3IT resources at the University of Zurich. We thank Y. Jing for patiently answering every question we had regarding their 2019 paper, and for sharing the data we requested. We also thank P. van Dokkum, J. Hudgings, D. Whitaker, D. Tanenbaum and R. Gaines for comments on an earlier draft, and C. Hayward for data-transfer support. J.M. thanks J.S.B., P.F.H., P. Torrey and L. Hernquist for sabbatical-leave hospitality. J.M. (an astronomer of Indigenous ancestry, non-Cherokee) thanks D. Ingram (a Cherokee physicist) for sharing knowledge about the Cherokee Nation and cultural appropriation. This work was conducted on Tongva-Gabrielino land.

Author contributions

J.M. conducted the analysis and designed the manuscript, with substantial input from S.D. and J.S.B. S.D. collected observational data from the literature and verified the theory–observations comparisons. R.F. ran the cosmological simulation used in this work. O.Ç. generated the halo catalogues and merger trees. A.G. provided support for the creation of mock images. A.L. and C.B.H. provided support with yt. C.K. calculated g-band effective radii, Sérsic indices and surface brightness contours. C.K. and F.J.M. calculated stellar ages, metallicities and colours; and S.D. conducted the observational comparison. J.S.B., R.F., O.Ç. and F.J.M. worked on the discussion of numerical stripping, with substantial input from F.J. Z.H. contributed

to the literature comparison. All authors contributed to the final creation of the manuscript and figures.

Competing interests
The authors declare no competing interests.

Additional information
Supplementary information The online version contains supplementary material available at https://doi.org/10.1038/s41550-021-01598-4.

Correspondence and requests for materials should be addressed to Jorge Moreno.

Peer review information *Nature Astronomy* thanks the anonymous reviewers for their contribution to the peer review of this work.